CrossMark

Structural characteristics and pyrolysis behaviors of huadian oil shale kerogens using solid-state ^{13}C NMR, Py-GCMS and TG

Yulong You[1] · Xiangxin Han[1] · Jianguo Liu[1] · Xiumin Jiang[1]

Abstract The chemical structure of fossil fuel has a significant effect on its pyrolysis. Present work studied the relevance of chemical structure and pyrolysis characteristics of three Huadian oil shale kerogens by using ^{13}C NMR, Py-GCMS and TG. ^{13}C NMR indicates aliphatic carbons are dominated in kerogen carbon skeleton and mainly in the form of straight methylene chains. Compared to kerogen of Dachengzi and Gonghe oil shale, kerogen of Gonglangtou oil shale has much higher branched degree of aliphatic chain, content of aromatic methyl and aromaticity. Distribution of fast pyrolysis products and thermal mass loss behaviors of kerogen are discussed with the correlation between the pyrolysis mechanism and chemical structure. The results of Py-GCMS show that main components of shale oil come from the structure of aliphatic carbons, especially methylene chains, and there is a clear correlation between content of aromatic products and aromaticity of kerogen. TG curves are fitted by a set of subcurves which represent various types of chemical bond cleavage during pyrolysis. The fitting results indicate mass loss mainly results from cleavage of bonds related to aliphatic carbons and difference of total mass loss is due to content of aliphatic carbons. The difference of mass loss at high temperature (500–1000 °C) is related to the bond cleavage of aromatic structure.

Keywords Kerogen · Chemical structure · Py-GCMS · TG analysis · Pyrolysis mechanism

✉ Xiumin Jiang
  xiuminjiang@sjtu.edu.cn

[1] Institute of Thermal Energy Engineering, School of Mechanical Engineering, Shanghai Jiao Tong University, Shanghai 200240, People's Republic of China

Introduction

Oil shale, a kind of fossil fuel containing organic matter called kerogen and inorganic minerals, is a significant alternative fossil fuel for current energy utilization. Pyrolysis is one of most common ways for oil shale utilization, and during this process, kerogen decomposes to release oil, gas and solid residue. To better control the thermal conversion of oil shale and obtain more valuable products we need is key issue of oil shale utilization. Therefore, thermal conversion mechanism of kerogen is of great significance in the research.

Kerogen is a kind of complex cross-linked organic matter which mainly contains C, H and O with relatively less N and S, and chemical bonds in kerogen are mainly involved with kinds of C–C bonds, C=C bonds, C–H bonds, C–O bonds, C–N bonds and C–S bond, where C atom can be aliphatic or/and aromatic carbon [1–3]. In molecular level, kerogen pyrolysis can be seen as cleavage and interaction of various chemical bonds in kerogen macromolecule [4, 5]. Therefore, a deeper understanding of kerogen chemical structure is quite important for exploring the pyrolysis behavior and formation mechanism of various products. With development of various measuring techniques [including solid-state ^{13}C nuclear magnetic resonance (NMR), Fourier transform infrared (FTIR), X-ray diffraction (XRD) and X-ray photoelectron spectroscopy (XPS)], researches on chemical structure of organic matter in kinds of fossil fuel, such as coal, biomass and oil shale, have been greatly improved. Kelemen et al. [6] used various methods to compare the structure characteristics of different types of kerogens. Tong et al. [3] comprehensively analyzed the carbon skeletal structure and heteroatomic functional groups of Huadian Dachengzi oil shale kerogen. These studies laid a foundation for constructing

kerogen macromolecule model, and with the help of theoretical methods, such as molecular dynamics and quantum chemistry, the pyrolysis process can be analyzed by simulation.

A large number of studies have been reported on the oil shale pyrolysis mechanism. For example, thermogravimetric (TG) analysis has been widely used in pyrolysis characteristics and kinetics [7–10]. In recent years, TG analyzer combined with mass spectrometry and/or Fourier transform infrared spectroscopy has become an effective way to explore the relationship between mass loss and release characteristic of products [11–13]. Fast pyrolysis techniques, such as Py-GCMS, have the advantage of reducing the second cracking reactions and obtaining the distribution of primary pyrolysis products as far as possible. Therefore, this method can be used to characterize the complex macromolecules of organic matter in fossil fuel [14–17]. Current researches on oil shale are mainly focused on the analysis of kerogen structure, the influence of operation conditions on pyrolysis behavior [13, 18–20], the effect of minerals on oil shale pyrolysis [11, 21] and co-pyrolysis characteristics of oil shale with other fossil fuels [22]. It is necessary to do more researches on the relevance of kerogen chemical structure and thermal conversion to further understand the mechanism of kerogen pyrolysis.

In this paper, several experiments have been carried out to study the chemical structure and pyrolysis behaviors of different Huadian oil shale kerogens in China. Solid-state ^{13}C NMR was used for the qualitative and quantitative analysis of carbon skeleton structure of kerogens. Pyrolyzer-gas chromatograph/mass spectrometer (Py-GCMS) was used for studying the pyrolysis characteristics and product distribution of kerogen fast pyrolysis. Thermogravimetric (TG) analysis was used to obtain mass loss behaviors of kerogen pyrolysis. Using kerogen as samples is aimed at eliminating the interference of inorganic minerals. Moreover, the relationship between chemical structure and decomposition of kerogen macromolecule is discussed.

Materials and methods

Samples

The three oil shale samples studied in this work were obtained from the 4th layer of Dachengzi mine (DCZ), the 11th layer of Gonglangtou mine (GLT) and the 4th layer of Gonghe mine (GH) located in Huadian city, China. The samples were treated by crush, grind and sieve to the size of 0–0.25 mm according to the National Standards of China (GB 474-1996). Then, the fine samples were demineralized with HCl/HF by the methods from references to gain kerogen [3, 23]. Demineralization process can be described briefly as follow. First, per 15 g prepared oil shale sample was added to 150 mL of 6 mol L^{-1} HCl solution and the mixture was stirred in a 70 °C water bath under a nitrogen atmosphere for 24 h. This mixture was filtered and washed with distilled water to make the filtrate became neutral. Then, the filter residue was dried at 110 °C under vacuum. Second, the pretreated samples were added 150 mL mixture of 6 mol L^{-1} HCl and 40 mass% HF in 1:1 ratio and treated with same ways as above.

The results of elemental analysis of three kerogens are shown in Table 1. According to classification based on the van Krevelen diagram of H/C versus O/C atomic element ratios [1], kerogen DCZ and GH are typical I kerogen which is usually very aliphatic, while kerogen GLT is II-III kerogen which contains higher content of aromatics.

Solid-state ^{13}C NMR

Solid-state ^{13}C NMR spectroscopic measurement for three kerogens was operated on a Bruker Avance III 400 NMR spectrometer at 100.63 MHz. The kerogen samples (200–300 mg) were located in a 4-mm-diameter zirconia rotor and spun at 5 kHz. A contact time and recycle delay time were set as 1.5 ms and 5 s, respectively, in the cross-polarization (CP) experiments. The acquisition time was 16 ms. [13]C chemical shifts measured were relative to the carboxyl carbon resonance of an external standard (glycine, GLY) at 176.03 ppm.

To obtain the quantitative information of different carbon types in three kerogen samples, the ^{13}C NMR spectrums were fitted according to the parameters of peaks, such as the ratios of Gaussian to Lorentz, the full width at half maximum (fwhm) and the chemical shifts (their respective values and assignments are referred to references [3, 5] and presented in Table 2).

Table 1 Elemental analysis of Huadian oil shale kerogens (mass%, dry ash free basis)

Sample	Kerogen DCZ	Kerogen GLT	Kerogen GH
C	72.17	65.43	72.16
H	9.48	6.03	9.16
O[a]	14.99	21.81	15.56
N	1.38	2.11	1.36
S[b]	1.98	4.62	1.76
H/C[c]	1.576	1.106	1.523
O/C[c]	0.156	0.25	0.162
Kerogen type	Kerogen I	Kerogen II-III	Kerogen I

[a] By difference; [b] Total sulfur; [c] Atomic ratio

Table 2 Distribution of structural carbons in solid-state ^{13}C NMR spectrum of Huadian kerogens

Carbon functionality	Symbol	Location	Chemical shift/ppm	Content/mol%		
				Kerogen DCZ	Kerogen GLT	Kerogen GH
Aliphatic methyl	f_{al}^1	—CH$_3$	14.4	1.64	2.70	1.05
Aromatic methyl	f_{al}^a	CH$_3$	19.8	1.73	5.79	1.38
Aliphatic C(2) carbon	f_{al}^2	—CH$_2$-CH$_2$-CH$_3$	25	9.98	9.75	11.63
Methylene	f_{al}^3	—CH$_2$-CH$_2$-CH$_2$—	30.2	68.62	29.40	64.96
			32.8	1.42	0.92	3.06
Methine	f_{al}^4	CH	38	0.11	1.80	0.21
Quaternary	f_{al}^5	C	42.1	0.29	4.72	0.56
Oxy-methylene	f_{al}^{O1}	—CH$_2$-O—	50–60	0.01	2.59	0.01
Oxy-methine	f_{al}^{O2}	C-O—	60–70	0.43	0.86	0.00
Oxy-quaternary	f_{al}^{O3}	C-O—	75–90	2.58	7.48	2.18
Ortho-oxyaromatic protonated	f_a^{O1}	CH	109.5	1.24	3.51	0.97
Ortho-oxyaromatic branched	f_a^{O2}	C	119.4	0.90	3.45	1.10
Aromatic protonated	f_a^H	CH	126	1.45	4.26	1.16
Aromatic branched	f_a^S	C	130–140	1.17	3.82	2.07
Bridging ring junction	f_a^B	C	132	1.45	3.68	1.39
Oxyaromatic	f_a^{O3}	C-O	150.3	2.28	3.37	2.46
Carboxyl	f_a^{CC1}	—COOH/R	175.5	3.71	9.59	4.55
Carbonyl	f_a^{CC2}	C	200–210	0.99	2.30	1.24

Py-GCMS

Fast pyrolysis experiments were conducted on a system combined with CDS5150 pyrolyzer, Agilent 7890 GC and 5975 MS. In each test, about 1 mg kerogen sample was pyrolyzed at 520 °C under Ar atmosphere (1.0 mL min^{-1}) and kept for 15 s to make the reaction completed. In the gas chromatograph, Ar was used as the carrier gas and the split ratio was 50:1. The column was 30 m Rxi-5MS capillary column (0.25 mm inner diameter, 0.25 μm film thickness). The temperature of the oven was held at 50 °C for 5 min, programmed to 250 °C at 5 °C min^{-1} and held for 5 min; then programmed to 300 °C and held for 3 min. Peak identification was done using the NIST11 mass spectrum library.
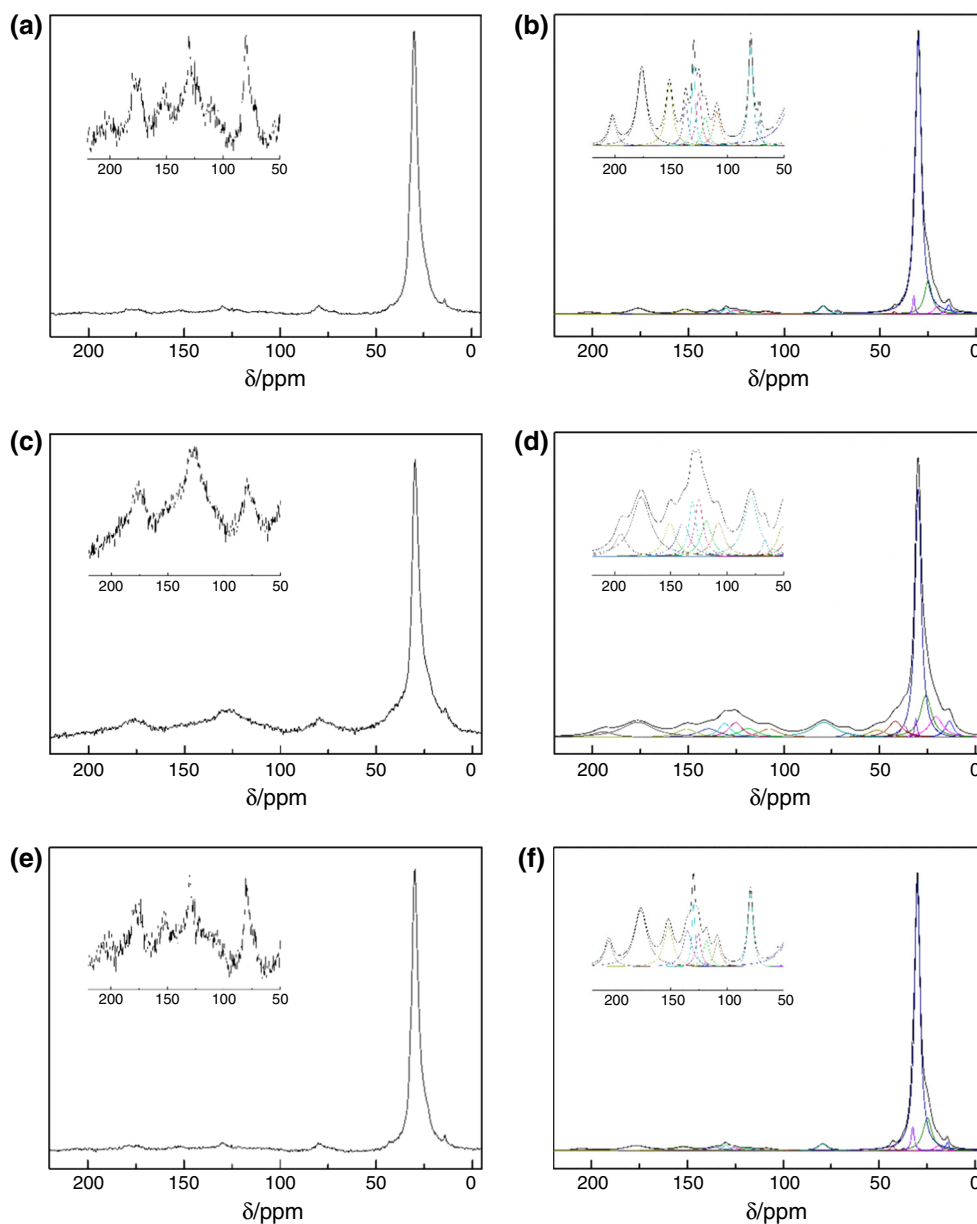
Fig. 1 Solid-state ^{13}C CP/MAS NMR spectrums and its fitting curves of Huadian kerogens. **a** Raw spectrum of kerogen DCZ. **b** Fitting spectrum of kerogen DCZ. **c** Raw spectrum of kerogen GLT. **d** Fitting spectrum of kerogen GLT. **e** Raw spectrum of kerogen GH. **f** Fitting spectrum of kerogen GH

TG analysis

TG analysis was performed by using a NETZSCH STA 449F3 thermal analyzer system coupled online with a Netzsch QMS 403 mass spectrometer and Bruker Vertex 70v FTIR spectrometer. The experiment was operated at heating rate of $10\ °C\ min^{-1}$ in a range from ambient temperature to $1000\ °C$ under Ar atmosphere of $50\ mL\ min^{-1}$. 10 mg kerogen was used per experiment.

Results and discussion

NMR results

The CP/MAS ^{13}C NMR spectrums and corresponding fitting curves present in Fig. 1 show that Huadian oil shale kerogens mainly contain aliphatic structure. Overall, spectrums of kerogen DCZ and kerogen GH are similar and mole percent of aliphatic carbons in these two kerogens is 86.80 and 86.03%, respectively. Kerogen GLT has relatively lower aliphatic structure with 59.10% of mole percent of aliphatic carbons. The main peaks of three kerogens

Table 3 Chemical structure parameters in Huadian kerogens

Structural parameter	Symbol	Definition	Kerogen DCZ	Kerogen GLT	Kerogen GH
Ratio of aliphatic carbon	f_{al}	$f_{al} = f_{al}^1 + f_{al}^a + f_{al}^2 + f_{al}^3 + f_{al}^4 + f_{al}^5 + f_{al}^O$	86.80%	66.01%	86.03%
Branched degree of aliphatic chain	BI	$BI = \frac{f_{al}^4 + f_{al}^5}{f_{al}}$	0.0046	0.0987	0.0090
Average methylene chain length	C_{acl}	$C_{acl} = \frac{f_{al}^2 + f_{al}^3}{f_a^S}$	59.67	7.94	32.89
Aromaticity	f_a	$f_a = f_a^{O1} + f_a^{O2} + f_a^{O3} + f_a^H + f_a^S + f_a^B$	8.49%	22.10%	9.15%
Average number of aromatic carbons per cluster	C_a		9.1	9.0	8.6
Coordination number	$\sigma + 1$	$\sigma + 1 = \frac{(f_a^{O3} + f_a^S)C_a}{f_a}$	3.71	2.93	4.25

centered in about 20–40 ppm indicate the domination of methylene carbons in carbon skeletons, but there are still large differences between the structural characteristics of three kerogens which can be obtained from detailed quantitative information. The content of aromatic methyl in kerogen GLT is far higher than that in kerogen DCZ and GH. Assuming all methylene carbons exist as straight chains in kerogen, and average methylene chain length, calculated from mole presents of methylene carbons divided by that of aromatic branched carbons [6], is 59.67 of kerogen DCZ, 7.94 of kerogen GLT and 32.89 of kerogen GH. However, methylene chain lengths may be lower than the values mentioned above because of the existence of saturated rings and branched chains in carbon skeletons. Peaks at 38 and 42 ppm are assigned to methane and quaternary carbons, and branched degree of aliphatic chain can be calculated by mole presents of methine and quaternary carbons divided by that of total aliphatic carbons. As shown in Table 3, branched degree of aliphatic chain is much higher in kerogen GLT, and branched degree in kerogen GH is about twice more than that in kerogen DCZ. Tong et al. [3] compared full width at half maximum of kerogens from Dachengzi, Nevada and Green River, and concluded the content of alicyclics in kerogen DCZ was very low. Therefore, short average methylene chain length in kerogen GLT can be thought to result from high aromaticity and branched degree of aliphatic structure, and difference of average methylene chain length between kerogen DCZ and GH is mainly due to branched degree of aliphatic structure although the content of aliphatic carbons is similar. Compared to kerogen DCZ and kerogen GH which mainly contain straight methylene aliphatic chains, there are more saturated rings and/or branched chains in aliphatic structure in kerogen GLT.

The resonance signals related to aromatic structures are distributed in 90–200 ppm. The average number of aromatic carbons per cluster in kerogen can be calculated by the method from Ref. [24], and the results shown in Table 3 indicate the aromatic carbons are in the form of 1- to 2-ring aromatic clusters. The coordination number [25] is used to describe the substitutive number of single aromatic cluster, and the results show that approximate 3–4 H atoms in per aromatic cluster are substituted by various functional groups or aliphatic chains. By contrast, substitutive degree of aromatic cluster in kerogen GH is highest, followed by that in kerogen DCZ and GLT.

Heteroatom structures detected in the ^{13}C NMR are mainly associated with oxygen-containing groups. Peaks between 50 and 90 ppm originate from aliphatic carbons linked to oxygen with different bonds, such as kinds of aliphatic alcohols and ethers. Peak in 175.5 ppm is assigned to carboxyl, and resonance signals at 200–210 ppm are corresponding to carbonyl. For the three Huadian kerogens, the content of carboxyl is higher than carbonyl. NMR results indicate higher content of oxygen-containing groups in kerogen GLT which are mainly in the form of carboxyl, carbonyl and quaternary oxygen.

Distribution of oil products

The GCMS chromatograms are shown in Fig. 2, and product distributions of kerogen pyrolysis are shown in Fig. 3. Several studies [20, 26, 27] have showed the optimum temperature for oil shale under fast pyrolysis is 520 °C, because kerogen may not decompose completely at lower temperature and excessively high temperature will cause gas-phase oil cracking reactions. In this work, pyrolysis temperature was set to 520 °C to ensure that pyrolysis products mainly come from kerogen primary decomposition. It is obvious that the product distributions of kerogen DZC and kerogen GH are basically similar, while that of kerogen GLT is quite different. Overall, except undefined components, pyrolysis products of kerogen DZC and kerogen GH mainly consist of oil components, and
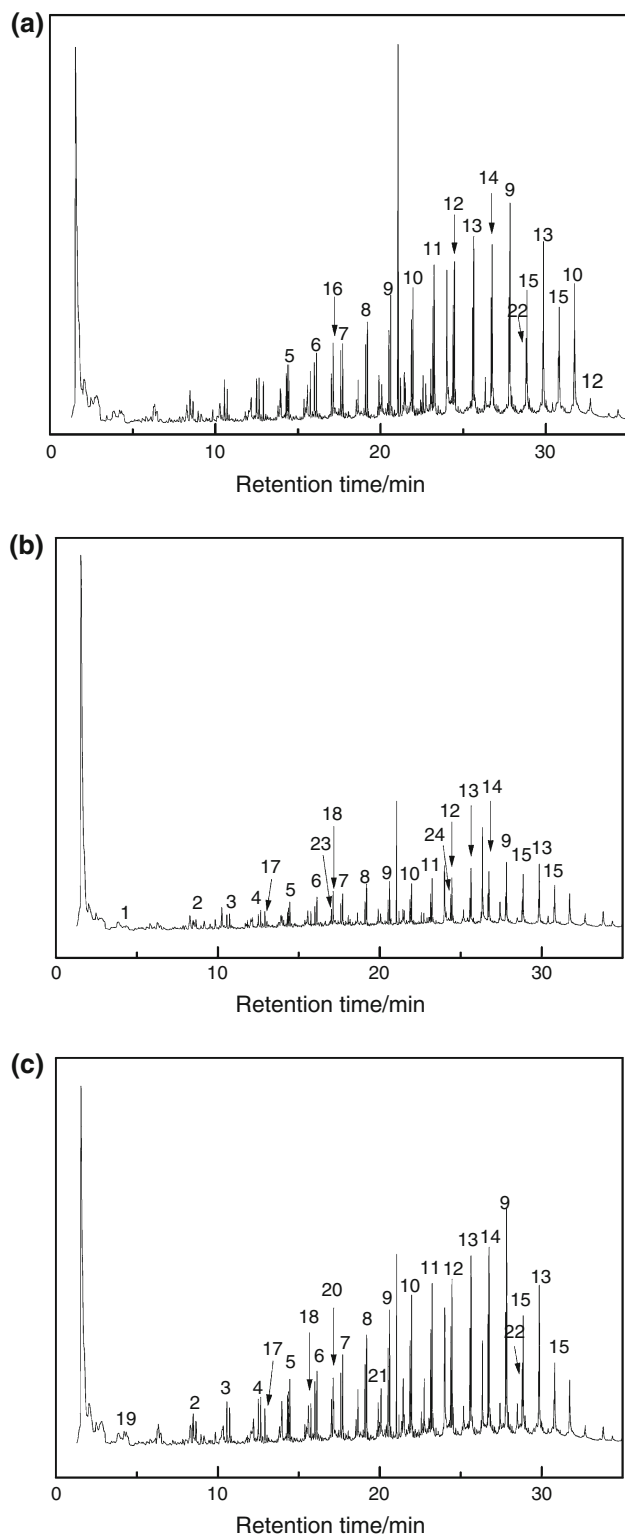
Fig. 2 Gas chromatograms of Huadian kerogens. a Kerogen DCZ. b Kerogen GLT. c Kerogen GH

products of kerogen GLT have more gas components. As expected, aliphatics originating from aliphatic structure are the majority components in oil products. It is worth noting
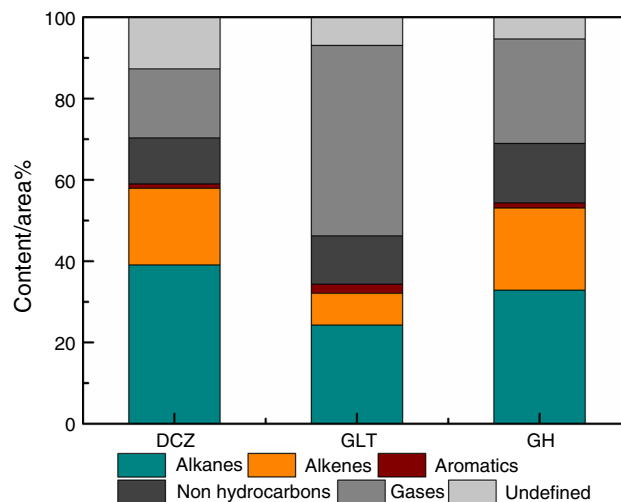
Fig. 3 Product distributions of kerogen pyrolysis

that kerogen GLT has the largest aromatic proportion though total oil content is significantly less than those of other two kerogens. It can be speculated that the relatively high aromaticity of kerogen GLT causes abundant aromatics in products. High content of gas components in products of kerogen GLT might be explained by following reasons. First, relatively short average methylene chain length in kerogen GLT indicates more aliphatic products with relatively less carbon numbers release as hydrocarbon gases rather than oil. And the higher content of aromatic methyl means more aliphatic carbons are release as CH_4 by removal of aromatic methyl [28]. Moreover, there are higher content of carboxyl and carbonyl which tend to release as CO_2 and CO in pyrolysis. Detailed analysis of distributions of oil components will be discussed in the following.

According to product chemical structure, aliphatics can be further classified into n-alkanes, cycloalkanes, branched alkanes and alkenes [4, 17]. Considering alkanes occupy a relatively large proportion in oil components, alkanes have been signed in Fig. 2, and corresponding products are listed in Table 4. It should be noted that there are some alkanes with same carbon number exiting in different peak positions, which is due to the existence of isomerides that cannot be distinguished well by GCMS. As Fig. 4 shows, the distribution of alkanes ranges from C8 to C24 and maintains a good continuity of carbon number. Alkanes are mainly concentrated between C17 and C24, accounting for 87.73, 77.25 and 81.19% in total alkanes of kerogen DCZ, GLT and GH, respectively.

Alkenes are basically consisted of mono-alkenes in Fig. 5. There was also few branched alkene, 7-methyl-6-tridecene, being detected in products of kerogen GLT and

Table 4 Product distribution of alkanes

	Product	Content/area%		
		Kerogen DCZ	Kerogen GLT	Kerogen GH
1	Octane		0.65	
2	Decane		0.43	0.56
3	Undecane		0.45	0.53
4	Dodecane		0.48	0.62
5	Tridecane	0.9	0.7	0.81
6	Tetradecane	0.95	0.64	0.88
7	Pentadecane	1.3	0.87	1.18
8	Hexadecane	1.53	1.02	1.4
9	Heptadecane	5.12	2.39	4.38
10	Octadecane	5.93	0.94	3.12
11	Nonadecane	2.3	1.07	1.94
12	Eicosane	3.52	1.56	2.11
13	Heneicosane	6.05	3.2	4.44
14	Docosane	3.13	1.36	2.63
15	Tetracosane	4.62	6.05	4.08
16	Hexadecane, 2,6,10,14-tetramethyl-	1.64		
17	Undecane, 2,6-dimethyl-		0.46	0.51
18	Dodecane, 2,6,10-trimethyl-		1	0.45
19	Hexane, 2,4-dimethyl-			0.96
20	Hexadecane, 2,6,10,14-tetramethyl-			0.94
21	Tridecane, 5-propyl-			0.45
22	Cyclotetracosane	1.15		0.87
23	Cyclotridecane		0.39	
24	Cycloeicosane		0.68	
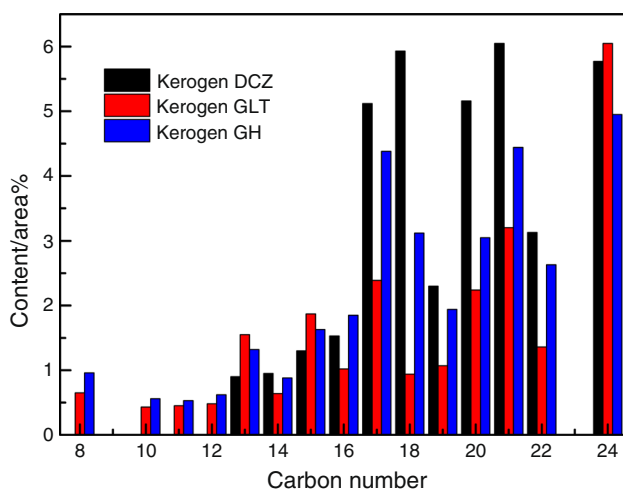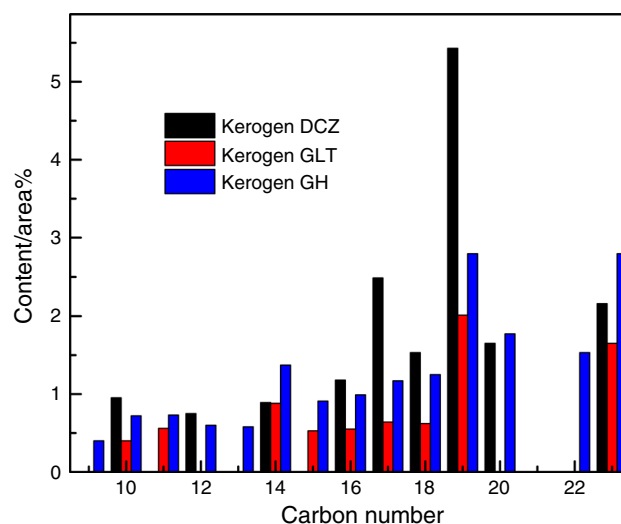
Fig. 5 Carbon number distributions of alkenes

GH. Formation of alkenes is thought to relate to alkanes. In pyrolysis, a long methylene chain cracks into an alkene and a shorter methylene chains and the latter will further crack or form an alkane by combining a H atom [29]. This mechanism can well explain the dominance of mono-alkenes in total alkenes and carbon number continuity of alkanes.

Branched alkanes and cycloalkanes detected in GCMS occupy 9.5% of kerogen DCZ, 12.81% of kerogen GLT and 12.72% of kerogen GH in total alkanes. The content of branched alkanes is quite higher than that of cycloalkanes in kerogen DCZ and GH as shown in Table 4. Huang et al. [17] studied the product distribution of Dachengzi oil shale during fast pyrolysis with different temperature, and the results indicated cycloalkanes were far more abundant than branched alkanes in high temperature. It was considered that cycloalkanes partly came from the saturated rings in original kerogen and partly resulted from the cyclization reactions of the alkanes and alkenes. According to NMR results, it can be concluded that higher branched degree of aliphatic chain in kerogen GH compared to kerogen DCZ causes the higher content and more variety of branched alkanes and cycloalkanes in products.

As shown in Table 5, the relationship of the yield of aromatics and kerogen chemical structure can be seen clearly in product distribution. High aromaticity leads to relatively abundant aromatic products of kerogen GLT. It is considered that C_{al}–C_{al} bonds at the β points are much easier to be cracked, and thus some methylenes will keep linking to aromatic rings [5]. This explains that there is relatively high content of benzene homologs with methyls detected in aromatic products. Meanwhile, abundant

Fig. 4 Carbon number distributions of alkanes

Table 5 Product distribution of aromatics

Product	Content/area%		
	Kerogen DCZ	Kerogen GLT	Kerogen GH
Benzene		0.49	0.41
Toluene	1.08		0.84
Benzene, 1,3-dimethyl-		0.44	
Bicyclo[4.2.0]octa-1,3,5-triene		0.71	
Benzene, 1,2,3-trimethyl-		0.58	

Table 6 Product distribution of heteroatomic compounds

Product	Content/area%		
	Kerogen DCZ	Kerogen GLT	Kerogen GH
Phenol		1.12	0.8
Phenol, 3-ethyl-			0.41
Phenol, 2-methyl-		0.46	
p-Cresol		1.07	
Octanoic acid	0.77		0.99
Nonenoic acid			0.51
Nonanoic acid	0.74	0.49	1.21
Decanoic acid	0.82	0.64	0.73
Undecylenic acid			0.39
Dodecanoic acid	0.81	0.46	0.81
Tridecanoic acid			0.74
Tetradecanoic acid	0.76		1.05
Pentadecanoic acid	0.76	0.42	0.95
Hexadecanoic acid	3.94	2.35	2.56
Heptadecanoic acid		0.46	0.52
Octadecanoic acid	0.86	3.4	1.6
Nonadecanoic acid		0.62	0.47
Eicosanoic acid			0.49
Bis(2-ethylhexyl) phthalate		0.41	

benzene homologs in aromatic products of kerogen GLT are also due to the high content of aromatic methyl.

Heteroatomic components studied in this work mainly refer to those compounds with oxygen-containing functional groups as shown in Table 6, which are consisted of various fatty acids and less phenols. In kerogen GLT, one kind of ester, Bis(2-ethylhexyl) phthalate, has been detected. Phenols are thought to be derived from oxygenated aromatic carbon [30] since the C_{ar}–O bond is quite thermally stable and will not break up under usual oil shale

pyrolysis temperature. According to NMR results, the mole percent of oxygenated aromatic carbon is 1.71% in kerogen DCZ, 6.88% in kerogen GLT and 2.87% in kerogen GH, respectively. The product of kerogen GLT contains the largest proportion of phenols and is followed by that of kerogen GH. There were no phenols detected in products of kerogen DCZ.

TG analysis

The TG results of three kerogens are present in Fig. 6. The total mass loss is 74.7% of kerogen DCZ, 55% of kerogen GLT and 75.2% of kerogen GH. Based on pyrolysis characteristics of oil shale and kerogen, the pyrolysis processes can be divided into three stages as shown in Fig. 6a. stage I corresponds to the temperature range of 180–350 °C and was involved with small amount of mass loss. And this stage is considered as transition from kerogen to bitumen [31]. Stage II, from 350 to 500 °C, is the majority of total mass loss for most of oil shales [10, 31, 32], which indicated severe decomposition of kerogen macromolecule. In stage III, from 500 to 1000 °C, there was still relatively distinct decline of TG curve of kerogen GLT with 10.32% mass loss, while kerogen DCZ and GH only had 5.16 and 4.85% mass loss, respectively. From the view of the change tendency of TG curves, there are sudden changes in the curves between stage II and III of kerogen DCZ and GH, while the curve shape there of kerogen GLT is relatively flat there. As mentioned above, pyrolysis process of fossil fuel, including oil shale, can be seen as cleavage of various chemical bonds and free radical reactions. Cleavage and reaction of chemical bonds are not only determined by the bond types but also affected by surrounding functional groups [4, 33]. And the mass loss during kerogen pyrolysis can be seen as macro reflection resulting from a serious of cleavage and arrangement of bonds in the molecular level. Peak fitting is widely used in kinetic studies on thermochemical conversion of coal and biomass by splitting result curve into different sub-curves to analyze integrated process which is consisted of multiple sub-procedures [34]. In this way, a DTG curve can be fitted by different sub-curves to correlate the pyrolysis behaviors with kerogen chemical bond reactions.

Figure 6 shows the DTG fitted results of three kerogens. In fitted curves, full width at half maximum was set to the value less than 200 °C, as listed in Table 7, meaning a standard deviation of Gaussian distribution (σ) of less than 85 °C [34]. Peak 1, with peak temperature from 320 to 360 °C, is likely related to release of carboxyl and ester and CO_2 formation [34]. The mass loss of kerogen GLT is relatively more obvious than other two kerogens in stage I, which can be ascribed to more formation of gas components, mainly CO_2.

Fig. 6 TG and DTG curves of Huadian kerogen. **a** TG curves of Huadian kerogen. **b** DTG curve of kerogen DCZ. **c** DTG curve of kerogen GLT. **d** DTG curve of kerogen GH
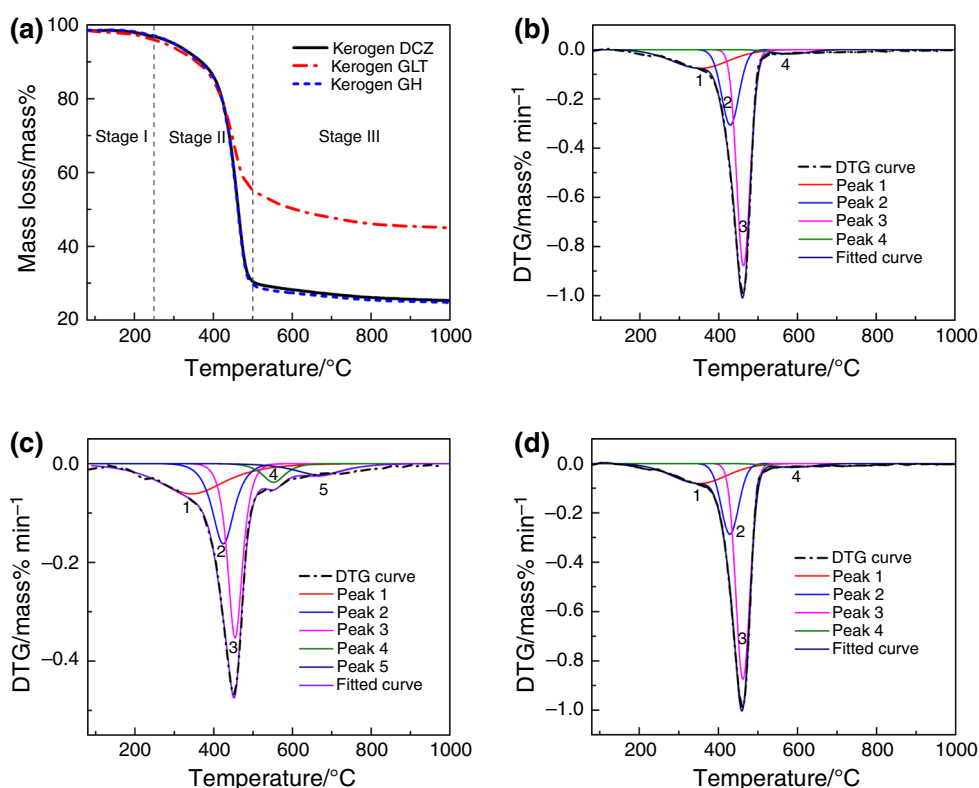
Peaks 2 and 3 are located in stage II and associated with a serious of bond cleavage related to aliphatic structure. The energy of bonds between C_{al} and heteroatoms is usually lower than that of C_{al}–C_{al} bonds [34]. Therefore, peak 2 is assigned to cleavage of bonds between C_{al} and O, S and N. The cleavage of C_{al}–S and C_{al}–N can release heteroatomic functional groups such as amino, sulfhydryl, sulfuryl and sulfinyl, and further result in formation of NH_3, H_2S and SO_2 [11, 35, 36]. C_{al}–O bonds can be in the form of ether bonds, carbonyl and hydroxyl existing in aliphatic structure. These oxygen-containing aliphatic bonds can potentially low activation energy of reaction and usually first crack in pyrolysis [4, 5]. Peak 3 is the main peak for kerogen pyrolysis and related to C_{al}–C_{al} bond cleavage. And these bond cleavage reactions can occur in straight methylene chains, branched chains and saturated rings, or at the β points of chains linked to aromatic clusters and cause kerogen decomposition and formation of molecular fragments with various sizes. Finally, these fragments which are small enough to evaporate from the solid particle will release as kinds of volatiles. Much experimental effort [12, 13, 37] on oil shale pyrolysis from different regions showed that main volatiles, including various aliphatics, aromatics and oxygen-containing non-hydrocarbons, basically released in the temperature from 400 to 500 °C, which is in agreement with assignments of peak 2 and peak 3. Theoretical analysis and simulation researches on bond cleavage during kerogen thermal decomposition also confirm rationality of these assignments [4, 5, 33]. Obviously, mass loss of kerogen mainly results from thermal decomposition of aliphatic structure, and the difference of total mass loss is related to the distinction of aliphatic carbon content.

Peaks 4 and 5 are mainly considered to be reaction with aromatic carbons. Peak 4 is considered to be the cleavage of C_{ar} with C_{al}, O and S [34] which causes release of some volatiles and mass loss. For example, removal of aromatic methyl results in the formation of CH_4. Researchers have found there may be two reaction paths [28]: dehydrogenation of methyl linked to aromatic ring occurs and H free radical adds to the aromatic ring in ipso position and then leads to demethylation; or demethylation occurs directly. These two paths are all involved in cleavage of C_{al}–C_{ar} bond. Peak 5 is assigned to condensation of aromatic clusters through cross-linking reaction which results in formation of H_2. Huang et al. [37] studied kerogen pyrolysis using TG-MS and detected intense generating process of H_2 above 600 °C, which is consistent with assignment of peak 5. Obviously, peak 4 was more remarkable in kerogen GLT compared to DCZ and GH, and peak 5 only existed in kerogen GLT. The difference of DTG curves in high temperature indicates more intense reactions of aromatic structure in kerogen GLT.

Table 7 Fitted results of DTG curves

	Kerogen DCZ	Kerogen GLT	Kerogen GH
Peak 1			
Tp/°C	353	344	351
fwhm/°C	167	200	162
Peak area/%	19.18	27.42	19.73
Peak 2			
Tp/°C	429	424	429
fwhm/°C	52	64	52
Peak area/%	24.11	23.89	22.42
Peak 3			
Tp/°C	462	454	462
fwhm/°C	40	44	42
Peak area/%	53.92	35.32	55.06
Peak 4			
Tp/°C	583	552	588
fwhm/°C	105	68	122
Peak area/%	2.79	5.82	2.79
Peak 5			
Tp/°C		668	
fwhm/°C		143	
Peak area/%		7.55	

Table 7 also lists peak areas of sub-curves. The peak area is considered as a measure of contribution of bond cleavage to mass loss and is related to the mass of volatile products [34]. For kerogen DCZ and GH, peak 2 and peak 3 occupying over 77% in total DTG curves indicate decomposition of aliphatic structure is the main process of kerogen pyrolysis. With the termination of release of volatiles from aliphatic structures, mass loss of kerogen tends to be slow. Relatively low area proportion of peak 3 in kerogen GLT reflects limited yields of aliphatics and relatively high contribution of other structures related to peak 4 and 5, which can be considered as aromatic structures and oxygen-containing functional groups. Therefore, the effect of release of volatiles from aliphatic structures on mass loss of kerogen GLT is small compared to other tow kerogens and the curve shape tends to be gentle.

Conclusions

In this paper, the chemical structures of three Huadian kerogens were investigated by solid-state ^{13}C NMR. Kerogen pyrolysis behaviors were studied by the methods of Py-GCMS and TG experiments. The following conclusions can be drawn:

Huadian kerogens are mainly composed of aliphatic carbons generally in the form of straight methylene chain and thus aliphatics originating from aliphatic structure constitute the majority of oil components. Aromatic structure is mainly in the form of 1- to 2- aromatic rings. Heteroatom structure is mainly related to oxygen-containing functional groups in carbon skeleton. And these structures are the source of various products in fast pyrolysis. Comparatively speaking, kerogen GLT has higher content of aromatic methyl, greater branched degree of aliphatic chain and more aromaticity in this kerogen results to abundant aromatic components in products. Main stage of kerogen pyrolysis is due to bond cleavage associated with aliphatic carbons, especially C_{al}–C_{al} bonds, and the difference of total mass loss results from distinction of content aliphatic structure. Mass loss of kerogen GLT in high temperature results from cleavage of bonds related to aromatic carbons.

References

1. Vandenbroucke M, Largeau C. Kerogen origin, evolution and structure. Org Geochem. 2007;38(5):719–833.
2. Lille Ü, Heinmaa I, Müürisepp AM, Pehk T. Investigation of kukersite structure using NMR and oxidative cleavage: on the nature of phenolic precursors in the kerogen of Estonian kukersite. Oil Shale. 2002;19(2):101–16.
3. Tong JH, Han XX, Wang S, Jiang XM. Evaluation of structural characteristics of Huadian oil shale kerogen using direct techniques (solid-state ^{13}C NMR, XPS, FT-IR, and XRD). Energy Fuel. 2011;25(25):4006–13.
4. Ru X, Cheng ZQ, Song LH, Wang HY, Li JF. Experimental and computational studies on the average molecular structure of Chinese Huadian oil shale kerogen. J Mol Struct. 2012;1030(51):10–8.
5. Liu XP, Zhan JH, Lai DG, Liu XX, Zhang ZJ. Initial pyrolysis mechanism of oil shale kerogen with reactive molecular dynamics simulation. Energy Fuel. 2015;29(5):2987–97.
6. Kelemen SR, Afeworki M, Gorbaty ML, Sansone M, Kwiatek PJ, Walters CC, Freund H, Siskin M. Direct characterization of kerogen By X-ray and solid-state ^{13}C nuclear magnetic resonance methods. Energy Fuel. 2008;21(3):1548–61.
7. Jiang XM, Cui ZG, Han XX, Yu HL. Thermogravimetric investigation on combustion characteristics of oil shale and high sulphur coal mixture. J Therm Anal Calorim. 2006;85:761–4.
8. Kok MV. Recent development in the application of thermal analysis techniques in fossil fuels. J Therm Anal Calorim. 2008;91:763–73.
9. Tiwari P, Deo M. Detailed kinetic analysis of oil shale pyrolysis TGA data. AIChE J. 2012;58(2):505–15.
10. Bai FT, Guo W, Lu XS, Liu YM, Guo MY, Li Q, Sun YH. Kinetic study on the pyrolysis behavior of Huadian oil shale via non-isothermal thermogravimetric data. Fuel. 2015;146:111–8.
11. Yan JW, Jiang XM, Han XX, Liu JG. A TG–FTIR investigation to the catalytic effect of mineral matrix in oil shale on the pyrolysis and combustion of kerogen. Fuel. 2013;104(2):307–17.

12. Tiwari P, Deo M. Compositional and kinetic analysis of oil shale pyrolysis using TGA–MS. Fuel. 2012;94(5):333–41.

13. Pan LW, Dai FQ, Li GQ, Liu S. A TGA/DTA-MS investigation to the influence of process conditions on the pyrolysis of Jimsar oil shale. Energy. 2015;86(1):749–57.

14. Harfi KE, Mokhlisse A, Chanâa MB. Yields and composition of oil obtained by isothermal pyrolysis of the Moroccan (Tarfaya) oil shales with steam or nitrogen as carrier gas. J Anal Appl Pyrol. 2000;56(2):207–18.

15. Iglesias MJ, Río JCD, Laggoun-Défarge F, Cuesta MJ, Suarez-Ruiz I. Control of the chemical structure of perhydrous coals; FTIR and Py-GC/MS investigation. J Anal Appl Pyrol. 2002;62(1):1–34.

16. Brebu M, Tamminen T, Spiridon I. Thermal degradation of various lignins by TG-MS/FTIR and Py-GC-MS. J Anal Appl Pyrol. 2013;104(11):531–9.

17. Huang YR, Han XX, Jiang XM. Comparison of fast pyrolysis characteristics of Huadian oil shales from different mines using Curie-point pyrolysis-GC/MS. Fuel Process Technol. 2014;128:456–60.

18. Williams PT, Ahmad N. Influence of process conditions on the pyrolysis of Pakistani oil shales. Fuel. 1999;78(6):653–62.

19. Nazzal JM. The influence of grain size on the products yield and shale oil composition from the pyrolysis of Sultani oil shale. Energy Convers Manag. 2008;49:3278–86.

20. Wang S, Jiang XM, Han XX, Tong JH. Effect of retorting temperature on product yield and characteristics of non-condensable gases and shale oil obtained by retorting Huadian oil shales. Fuel Process Technol. 2014;121(1):9–15.

21. Ballice L. Effect of demineralization on yield and composition of the volatile products evolved from temperature-programmed pyrolysis of Beypazari (Turkey) Oil Shale. Fuel Process Technol. 2005;86(6):673–90.

22. Jiang XM, Cui ZG, Han XX, Yu HL. Thermogravimetric investigation on combustion characteristics of oil shale and high sulphur coal mixture. J Therm Anal Calorim. 2006;85:761–4.

23. Ballice L. Stepwise chemical demineralization of Göynük (Turkey) oil shale and pyrolysis of demineralization products. Ind Eng Chem Res. 2006;45(3):906–12.

24. Solum MS, Pugmire RJ, Grant DM. ^{13}C solid-state NMR of argonne premium coals. Energy Fuel. 1989;3(2):187–93.

25. Grant DM, Pugmire RJ, Fletcher TH, Kerstein AR. Chemical model of coal devolatilization using percolation lattice statistics. Energy Fuel. 1989;3(2):175–86.

26. Williams PT, Nazzal JM. Polycyclic aromatic compounds in oils derived from the fluidized bed pyrolysis of oil shale. J Anal Appl Pyrol. 1995;35(2):181–97.

27. Sadiki A, Kaminsky W, Halim H, Bekri O. Fluidised bed pyrolysis of Moroccan oil shales using the hamburg pyrolysis process. J Anal Appl Pyrol. 2003;70(2):427–35.

28. Jianbo J, Fangui Z, Meifen L, Kechang X. Mechanism of methane formation during toluene pyrolysis using DFT calculation. CIESC J. 2010;61(12):3235–42.

29. Rebick C. Pyrolysis: theory and industrial practice. New York: Academic Press; 1983.

30. Yan LJ, Bai YH, Zhao RF, Li F, Xie KC. Correlation between coal structure and release of the two organic compounds during pyrolysis. Fuel. 2015;145(145):12–7.

31. Li QY, Han XX, Liu QQ, Jiang XM. Thermal decomposition of Huadian oil shale. Part 1. Critical organic intermediates. Fuel. 2014;121(2):109–16.

32. Wang W, Li SY, Yue CT, Ma Y. Multistep pyrolysis kinetics of North Korean oil shale. J Therm Anal Calorim. 2015;119:643–9.

33. Guan XH, Wang D, Wang Q, Chi MS, Liu CG. Estimation of various chemical bond dissociation enthalpies of large-sized kerogen molecules using DFT methods. Mol Phys. 2016;114(11):1705–55.

34. Shi L, Liu QY, Guo XJ, Wu WZ, Liu ZY. Pyrolysis behavior and bonding information of coal—a TGA study. Fuel Process Technol. 2013;108(6):125–32.

35. Burnham AK, Taylor RW. Occurrence and reactions of oil shale sulfur. 15th oil shale symposium, Golden. Colo. 1982.

36. Oh MS, Taylor RW, Coburn TT, Crawford RW. Ammonia evolution during oil shale pyrolysis. Energy Fuel. 2002;32(1):100–5.

37. Huang YR, Fan C, Han XX, Jiang XM. A TGA-MS investigation of the effect of heating rate and mineral matrix on the pyrolysis of kerogen in oil shale. Oil Shale. 2016;33(2):125–41.